Published in final edited form as:
*Acta Biomater*. 2012 July ; 8(7): 2483–2492. doi:10.1016/j.actbio.2012.03.019.

# Development of silk-based scaffolds for tissue engineering of bone from human adipose derived stem cells

**Cristina Correia**[a,b,c], **Sarindr Bhumiratana**[a], **Le-Ping Yan**[b,c], **Ana L. Oliveira**[b,c], **Jeffrey M. Gimble, Ph.D.**[d], **Danielle Rockwood**[e], **David L. Kaplan**[e], **Rui A. Sousa**[b,c], **Rui L. Reis**[b,c], and **Gordana Vunjak-Novakovic**[a]

[a]Department of Biomedical Engineering, Columbia University, New York, NY, USA

[b]3B's Research Group – Biomaterials, Biodegradables and Biomimetics, University of Minho, Headquarters of the European Institute of Excellence on Tissue Engineering and Regenerative Medicine, Guimarães, Portugal

[c]ICVS/3B's - PT Government Associate Laboratory, Braga/Guimarães, Portugal

[d]Pennington Biomedical Research Center, Louisiana State University System, Baton Rouge, LA, USA

[e]Department of Biomedical Engineering, Tufts University, 4 Colby Street, Medford, MA, USA

## Abstract

Silk fibroin is a potent alternative to other biodegradable biopolymers for bone tissue engineering (TE), because of its tunable architecture and mechanical properties, and demonstrated ability to support bone formation, in vitro and in vivo. In this study, we investigated a range of silk scaffolds for bone TE using human adipose-derived stem cells (hASC), an attractive cell source for engineering autologous bone grafts. Our goal was to understand the effects of scaffold architecture and biomechanics and use this information to optimize silk scaffolds for bone TE applications. Silk scaffolds were fabricated using different solvents (aqueous vs. hexafluoro-2-propanol - HFIP), pore sizes (250–500μm vs. 500–1000μm) and structures (lamellar vs. spherical pores). Four types of silk scaffolds combining the properties of interest were systematically compared with respect to bone tissue outcomes with decellularized trabecular bone (DCB) included as a "gold standard". The scaffolds were seeded with hASC and cultured for 7 weeks in osteogenic media. Bone formation was evaluated by cell proliferation and differentiation, matrix production, calcification and mechanical properties. We observed that 400–600μm porous HFIP-derived silk fibroin scaffold demonstrated the best bone tissue formation outcomes as evidenced by increased bone protein production (osteopontin, collagen type I, bone sialoprotein), enhanced calcium deposition and total bone volume. On a direct comparison basis, alkaline phosphatase activity (AP) at week 2, and new calcium deposition at week 7 were comparable to the cells cultured in DCB. Yet, among the aqueous-based structures, the lamellar architecture induced increased AP activity and demonstrated higher equilibrium modulus than the spherical-pore scaffolds. Based on the collected data, we propose a conceptual model describing the effects of silk scaffold design on bone tissue formation.



*Corresponding author: Dr. Gordana Vunjak-Novakovic, Laboratory for Stem Cells and Tissue Engineering, Department of Biomedical Engineering, Columbia University, 622 W168th St, Vanderbilt Clinic 12-234, New York, NY 10032, Tel: 212-305-2304, gv2131@columbia.edu.

**Keywords**

Bone; Tissue engineering; Silk; Scaffold; Adipose stem cells

## 1. Introduction

Numerous approaches have been made towards development of an “ideal” scaffold for bone tissue engineering[1, 2]. Silk fibroin, obtained from silk-worms, demonstrates great biocompatibility along with outstanding mechanical properties [3] and proteolytic degradation [4]. In tissue engineering, silk fibroin has been extensively used for multiple types of scaffolds [5–8]. Various modifications of silk scaffolds have been fabricated with a wide range of chemical, structural and biomechanical modifications [6, 9, 10]. Silk sponges have been used for cartilage [11–13], fat [14, 15], silk tubes for blood vessels [16] and silk fibers for ligaments [17, 18]. Porous sponge scaffolds were suitable for bone tissue formation, by enhancing cell attachment, proliferation and migration. In addition, the high porosity (92–98%)[19–21] facilitates nutrient and waste transport into and out of the scaffolds.

Porous silk sponges can be fabricated using porogens, gas foaming, or lyophilization methods [22, 23]. Among these, NaCl salt leaching is among the simplest and most effective fabrication methods, resulting in scaffolds with spherical-shaped pores and different morphologies. Silk scaffolds are generally fabricated using two different silk preparation methods: aqueous- and solvent (HFIP)-based. HFIP does not solubilize salt particles, therefore pore sizes in these sponges reflect the size of the porogen used in the process [22, 23]. On the other hand, aqueous-based silk sponges demonstrate pore sizes 10–20% smaller than the size of salt crystals. This is due to partial solubilization of the surface of the salt particles during supersaturation of the silk solution before solidification [3, 24]. This partial solubilization results in rougher surfaces of the pores, which improved cell attachment [22, 25]. For comparison, aqueous-based processing results in sponges with higher porosity [22, 25], and higher degradation rates [22, 25].

Besides silk sponges with spherical-shaped pores, our laboratory developed a novel silk scaffold fabrication method to produce lamellar-like structure using a freeze drying technique [26]. This structure mimics bone lamellae structure. Human bone marrow mesenchymal stem cells, cultured on osteogenic media, attached, proliferated and assembled new extracellular matrix on this patterned structure [26].

Tissue engineers have explored silk scaffolds for bone regeneration by using bone marrow mesenchymal stem cells (BM-MSC) as the preferred cell source with superior outcomes validated with both aqueous-based [19, 26, 27] and HFIP-derived scaffolds [6, 21, 28]. Human adipose derived stromal/stem cells (hASCs), on the other hand, present features comparable to BM-MSC and are a promising alternative for cell based therapies [29] such as bone tissue regeneration. hASCs may be easily isolated from adipose tissue with a high yield of cells per unit tissue volume [30]. Furthermore, hASCs proliferate quickly, and their osteogenic potential is comparable to that of bone marrow mesenchymal stem cells [31]. Our research group has engineered half-centimeter–sized bone constructs *in vitro* by using human adipose-derived stem cells (hASCs) that were seeded in decellularized bone scaffolds and cultured dynamically in perfusion bioreactors [32].

Still, silk scaffold and hASCs are two potential components for bone tissue engineering applications, which have not been yet investigated in combination. In this study, five different scaffolds were investigated: 1) aqueous, spherical-pore structure, small pores (250–500 μm), and 2) aqueous, spherical-pore structure, large pores (500–1000 μm); 3) aqueous,

lamellar structure, 4) HFIP, medium pore sizes (400–600 μm), and 5) decellularized bovine trabecular bone used as a "gold standard", to evaluate hASCs osteogenic responses and bone tissue development.

## 2. Materials and Methods

### 2.1. Preparation of silk fibroin scaffolds

All chemicals were purchased from Sigma-Aldrich (St. Louis, MO) unless otherwise stated. Silk scaffolds were prepared according to Figure 1. Silk fibroin from silkworm (*Bombix mori*) cocoons was extracted with 0.02 M sodium carbonate ($Na_2CO_3$) solution, rinsed in distilled water, dissolved in a 9.3 M lithium bromide (LiBr) solution and dialyzed for 48h against distilled water in benzoylated dialysis tubing (Sigma D7884). Dissolved silk fibroin was centrifuged for 20 min at 9000 rpm (4°C). The resulting solution was determined by weighing the remaining solid after drying, yielding a 6-wt % aqueous silk fibroin solution.

Aqueous-derived silk fibroin porous sponges were prepared by salt leaching methods. NaCl salt was sieved with metal mesh to obtain particle size distributions between 250–500 μm (Aq-250), or 500–1000 μm (Aq-500), and added into silk fibroin aqueous solution at a 2:1 (w/v) ratio, in disk-shaped containers. The container was covered and left at room temperature. After 24h, the container was immersed in water to extract NaCl salt for 2 days with water changes.

Aqueous-derived silk fibroin lamellar scaffolds (Aq-Lam) were prepared by pouring silk fibroin aqueous solution into silicon tubing (6 mm i.d.), frozen at −80°C, lyophilized for 1 day, and autoclaved to induce the formation of β-sheet structure and insolubility in aqueous solution.

HFIP-derived silk fibroin scaffolds (HFIP-400) were prepared as previously described [25]. Silk fibroin aqueous solution was lyophilized and further dissolved with HFIP, resulting in a 17-wt % HFIP-derived silk fibroin solution. Granular NaCl particles (400–600 μm) were added to 2 mL of silk fibroin in HFIP at 2:1 (w/v) ratio. The containers were covered overnight to reduce evaporation of HFIP and to provide sufficient time for homogeneous distribution of the solution. Subsequently, the solvent was evaporated at room temperature for 3 days. The matrices were then treated in 90% (v/v) methanol for 30 min, to induce the formation of the β-sheet structure, followed by immersion in water for 2 days to remove NaCl porogens. Porous silk scaffolds were then freeze-dried. All scaffolds were cut and cored into cylinders of 4 mm in diameter and 2 mm thickness.

### 2.2. Preparation of trabecular bone scaffolds

Trabecular bone scaffolds were decellularized as in our studies [32, 33]. Trabecular bone cylinders (4 mm diameter) were cored from the subchondral region of carpometacarpal joints of bovine calves, and washed with a high velocity stream of water to remove bone marrow from pore spaces. Scaffolds were further washed for 1h in phosphate-buffered saline (PBS) with 0.1% ethylenediamine tetraacetic acid (EDTA) at room temperature (RT), followed by sequential washes in hypotonic buffer (10 mM Tris and 0.1% EDTA) overnight at 4 °C, in detergent (10 mM Tris and 0.5% sodium dodecyl sulfate) for 24 h at RT, and in enzyme solution (100 U/mL DNAse, 1 U/mL RNAse, and 10 mM Tris) for 6 h at 37 °C, to fully remove cellular material. Scaffolds were then rinsed in PBS, freeze-dried, and cut into 2 mm thick cylindrical plugs. The scaffolds within the density range of 0.28–0.38 $mg/mm^3$ (calculated based on the dry weights and exact dimensions) were selected for experiments.

### 2.3. Isolation, characterization and expansion of hASCs

hASCs were isolated according to previously described methods [34] from liposuction aspirates obtained from the Pennington Biomedical Research Center, under protocols approved by the Institutional Review Board. hASCs were expanded to the fourth passage in expansion medium: high-glucose Dulbecco's modified Eagle's medium (DMEM) supplemented with 10% fetal bovine serum (FBS), penicillin–streptomycin (1%), and 1 ng/mL basic fibroblast growth factor (bFGF).

Passage zero (P0) cells were examined for surface marker expression using flow cytometry. The presence of specific antigens such as CD29, CD105, CD45, CD34, CD44, CD73 and CD90 were analyzed, as previously published [34, 35]. hASCs were confirmed for their differentiation capacity into the adipogenic and osteogenic lineages in monolayer cultures following induction with adipogenic and osteogenic inductive medium for up to 14 days and histochemical analysis of neutral lipid (Oil Red O) or mineralization (Alizarin Red) staining as published [36].

Three independent series of experiments were performed, each with triplicates of samples for each experimental group, data point and analytical method.

### 2.4. Construct seeding and culture

All scaffolds were sterilized in 70% ethanol overnight, washed in PBS and incubated in expansion medium 24h prior to seeding. For construct seeding, expanded P4 hASCs were suspended in culture medium at $30\times10^6$ cells/mL. Scaffolds were blot-dried, placed individually into wells of a nontreated 12-well cell culture plate and a 20 μL aliquot of cell suspension was pipetted into each scaffold, and pipetted up and down to ensure even distribution of cells. After 15 minutes in the incubator, scaffolds were rotated 180°, and 10 μL of cell-free medium was added to maintain hydration. This process was repeated four times, to achieve uniform cell distribution, after which, osteogenic media (low glucose DMEM, 10% FBS, 1% penicillin–streptomycin, 10 mM sodium-b-glycerophosphate, 10 mM HEPES, 100 nM dexamethasone and 50 μg/mL ascorbic acid-2-phosphate) was added. hASC-seeded scaffolds were maintained in static culture (nontreated 12-well cell culture plate) and nourished with 3 mL of osteogenic media/well for 7 weeks to induce osteogenic differentiation of the stem cells, and ensure robust bone tissue development.

### 2.5. Live/Dead assay

LIVE/DEAD Viability/Citotoxicity kit (Molecular Probes, OR/USA) was used to evaluate cell viability. Live cells (indicated by calcein AM) and dead cells (indicated by ethidium homodimer-1) were observed and imaged through a confocal microscope (Leica, Germany). Optical surfaces were taken from the surface up until 160 μm deep, with 10 μm intervals. All images are presented as vertical projections.

### 2.6. Biochemical characterization

Constructs were harvested, washed in PBS, cut in half and weighed. For DNA assay, one-half was added to 1 mL of digestion buffer (10 mM Tris, 1 mM EDTA, 0.1% Triton X-100, 0.1 mg/mL proteinase K) and incubated overnight at 56°C for digestion. After centrifugation at 3000g, during 10 minutes, the supernatants were removed, diluted, pippeted in duplicate into a 96-well plate and 1:1 ratio (v/v) of Picogreen solution (Quant-iT™ PicoGreen® dsDNA Kit, Invitrogen) was added. Sample fluorescence was measured with fluorescent plate reader at excitation of ~480 nm, emission of ~520 nm. Lambda DNA was used to prepare the standard curve. Based on previous studies [32], 5 pg DNA/cell was used as the conversion factor to determine the cell number. For calcium quantification, one-half of constructs were incubated in 1 mL TCA 5% (trichloroacetic acid 5% v/v) and calcium was

extracted by disintegrating the construct using steel balls and MinibeadBeater™ (Biospec, Bartlesville, OK/USA). Calcium content and standard were quantified using StanbioTotal Calcium Liquicolor® (Stanbio Laboratory/USA). Sample optical density was measured at 575 nm using a microplate reader. Alkaline Phosphatase (AP) activity was determined by adding cell lysis solution to one-half of each scaffold, and these were disintegrated using steel balls and MinibeadBeater™. After centrifugation, 50 μL of supernatant were incubated with 50 μL *p*NPP (p-nitrophenyl-phosphate) substrate solution, at 37°C for 20 min. The reaction was stopped with 50 μL of stop solution, and absorbance was read at 405 nm. p-Nitrophenol at known concentrations was used to prepare the standard curve. All solutions were components of SensoLyte® *p*NPP Alkaline Phosphatase Complete Kit (Cell Biolabs, CBA-302).

### 2.7. Histology and Immunohistochemistry

After harvest, the samples were fixed in 4% formaldyhyde solution for 1 day. Bone scaffolds were decalcified with immunocal solution (Decal Chemical, Tallman, NY) for 1 day, and further dehydrated with graded ethanol washes, concurrently with remaining silk constructs. Samples were embedded in paraffin, sectioned to 5-μm slices and mounted on glass slides. For staining, sections were deparaffinized with CitriSolv and rehydrated with a graded series of ethanol washes. Samples were stained using standard hematoxylin and eosin. Immunohistochemistry was performed on sections as follows: sections were blocked with normal horse serum (NHS), stained sequentially with primary antibody (rabbit anti-human Osteopontin (OPN) polyclonal antibody, Chemicon ab1870; rabbit anti-bone sialoprotein (BSP) polyclonal antibody, Millipore ab1854; mouse monoclonal to Collagen I, Abcam ab6308; NHS for negative control), secondary antibody (Vectastain Universal Elite ABC Kit, PK-6200 Vector Laboratories) and developed with biotin-avidin system (DAB substrate kit SK-4100 Vector Laboratories).

### 2.8. Microcomputed tomography (*μ*CT) analysis

Before culture, the architecture of the silk scaffolds was evaluated using a micro-CT Skyscan 1072 scanner (Skyscan, Kontich, Belgium). The X-ray scans were acquired in high-resolution mode with a pixel size of 8 μm, an integration time of 1.3 s and with penetrative X-rays of 35 keV and 209 μA. Data sets were reconstructed using standardized cone-beam reconstruction software (NRecon v1.4.3, SkyScan). Representative data set of the slices was segmented into binary images with a dynamic threshold of 40–255 (grey values), which were used for morphometric analysis (CT Analyser, v1.5.1.5, SkyScan) and to build the 3D models (ANT 3D creator, v2.4, SkyScan).

After culture μCT was performed using the protocol described by Liu et al [37]. Samples were aligned in a 2 mL screw-cap centrifuge tube, which was clamped in the specimen holder of a vivaCT40 system (SCANCO Medical AG, Basserdorf, Switzerland). The 2 mm length of the scaffold was scanned at 21 μm isotropic resolution. A global thresholding technique, which only detects mineralized tissue, was applied to obtain the bone volume (BV) of samples.

### 2.9. Scanning electron microscopy (SEM)

Samples were washed in PBS and then fixed in 2% glutaraldehyde in sodium cacodylate buffer for 2 h. Constructs were washed in buffer and freeze-dried overnight. The samples were coated with gold and palladium and imaged in SEM machine (JEOL, JAPAN).

### 2.10. Mechanical testing

Young's modulus upon compression of constructs after culture was determined under unconfined compression in wet conditions using a modification of an established protocol [38]. An initial tare load of 0.2 N was applied and was followed by a stress-relaxation step where specimens were compressed at a ramp velocity of 1% per second up to 10% strain and maintained at the position for 1800 s. The Young's modulus was obtained from the equilibrium forces measured at 10% strain.

### 2.11. Statistical analysis

Data are presented as average (three independent series of experiments, each with n=3 per group, data point and analytical assay) ± standard deviation. Statistical significance was determined using analysis of variance (ANOVA) followed by Tukey's HSD (honestly significant difference) test using Prism software (Prism 4.0c, GraphPad Software Inc.).

## 3. Results

### 3.1. Characterization of undifferentiated hASCs

The immunophenotype of undifferentiated hASCs was evaluated using flow cytometry (Fig. 2A). The antigen expression profile observed was consistent with our previous study [39]: expression of adhesion molecules integrin β1 (CD29) and endoglin (CD105), high expression of ecto 5′ nucleotidase (CD73) surface enzyme as well as extracellular matrix proteins such as Thy-1 (CD90) and glycoprotein CD34. Hyaluronate (CD44) receptor molecule was less expressed than expected, however, expression of hematopoietic marker CD45 was accordingly very low. Multilineage potential of hASCs was evaluated by cultivation of cell monolayers in adipogenic or osteogenic medium. The isolated hASCs exhibited multi lineage differentiation as shown with formation of Oil Red O staining lipid droplets (Fig. 2C) and Alizarin Red staining extracellular mineralization (Fig. 2D).

### 3.2. Characterization of silk fibroin scaffolds

Aqueous-based silk fibroin scaffolds' architecture was characterized by SEM and μCT analysis (Fig. 3). Both SEM imaging (Fig. 3 Top) and micro-CT 3D reconstructions (Fig. 3 Middle) demonstrate the pore morphology of the developed structures. Spherical interconnected pores, forming a trabecular-like network, are observed in Aq-250 and Aq-500 groups, fabricated by salt-leaching method with 2 ranges of porogen sizes (250–500μm and 500–1000μm respectively). On the other hand, Aq-Lam presents a structure where the pore walls do not form a sphere, but parallel lamellae, which are aligned in several directions within the 3D structure. Porosity, interconnectivity, pore size and trabeculae thickness were obtained by μCT analysis (Fig. 3 Bottom): Aq-500 structure present the highest porosity value (86.62 % ± 0.84), and average pore size (254.32 μm ± 13.64), which is explained by the use of bigger NaCl particles. The highest percentage of interconnectivity (97.83 % ± 0.61) was also measured for this group. Aq-Lam characterization demonstrated a more compact structure, with lower porosity (64.25 % ± 8.82) and smaller pore size (126.24 % ± 48.16), and 35% lower pore interconnectivity (63.25 % ± 21.13) than Aq-500.

### 3.3. Cell viability and proliferation

Cell seeding efficiency, calculated as a fraction of the initial cells detected in the scaffold after seeding, ranged from 60 to 75% in all five groups, without statistically significant differences (Fig. 4A). DNA assay (Fig. 4B) demonstrated that, after two weeks of culture, proliferation occurred to the same extent (approximately 1.6-fold increase in cell numbers) in all spherical porous silk sponges, either aqueous or HFIP-based (Aq-250, Aq-500,

HFIP-400). In contrast, the lamellar structure maintained the initial cell numbers throughout the culture period. In aqueous scaffolds, the cell numbers achieved by week 2 were maintained through week 7. In HFIP scaffold group, the cell number increased continuously. In the decellularized bone group, the cell numbers decreased at the end of culture period. Live/Dead assay confirmed cell viability and attachment throughout all scaffolds (Fig. 4C).

Good distribution of cells at periphery and center of the constructs was observed through H&E staining in all groups (Fig. 5 top). Cells attached to scaffold surfaces, and filled the pore spaces. Rough pore surfaces were observed by H&E staining (Fig. 5 top) and SEM (Fig. 5 middle and bottom) in aqueous spherical-pore scaffolds in contrast to smooth pore surfaces in HFIP scaffolds. Matrix density appeared greater in aqueous porous scaffolds (Aq-250 and Aq-500) and the trabecular bone scaffold than in HFIP-derived scaffolds.

### 3.4. Bone tissue development

Distribution of bone tissue matrix was evaluated through immunolocalization of bone matrix proteins after 7 weeks of culture in osteogenic media. The expression of osteopontin (OPN), bone sialoprotein (BSP) and collagen type I (Col I) were similar in both small (Aq-250) and large (Aq-500) pore size aqueous silk sponges (Fig. 5). These bone matrix markers were distributed throughout the decellularized bone scaffold. The most robust groups were the aqueous lamellar and HFIP-derived sponges, with high intensity of immunolocalization of OPN and BSP, and somewhat lower intensity of collagen type I. The cells maintained their osteogenic properties throughout the duration of culture.

### 3.5. Quantification of bone differentiation parameters

To complement immunostains shown in Figure 5, quantitative biochemical data were obtained to determine the amounts of bone differentiation markers. Alkaline phosphatase (AP) activity, an early marker of osteoblastic phenotype peaked after 2 weeks of culture, as expected, at similar levels in all groups, except for the significantly higher expression in the Aq-Lam group (Fig. 7A). As an indicator of ECM maturation and calcification, AP activity levels decreased by seven weeks of culture. The calcium deposition increased in parallel to the decrease in AP activity, between weeks 2 and 7, with significantly higher levels in HFIP and decellularized bone scaffolds than in other groups (Fig. 7B). Consistent with the biochemically measured calcium levels, the bone volume (BV) detected by μCT analysis was also higher is HFIP than aqueous scaffolds and the highest in the decellularized bone group (Fig 7C). Although not significantly different, HFIP-derived sponges (HFIP-400) demonstrated increased bone volume relative to aqueous-based groups. The equilibrium modulus of the constructs was also highest for the decellularized bone group, and higher for the HFIP than aqueous spherical-porous scaffolds (Fig. 7D). Interestingly, the aqueous-based silk fibroin lamellar structure (Aq-Lam) was 3x stiffer than the corresponding aqueous-based porous silk sponges (Aq-250 and Aq-500) ($p<0.01$). This is evidence of the importance of the scaffold architecture for the resulting mechanical properties of engineered tissue. Furthermore, the mineralized tissue was better distributed in HFIP-400 group (Fig. 7E), where small spherical-like structures were observed, whereas in aqueous groups, mineral deposited less uniformly throughout the construct, forming plate-like structures.

## 4. Discussion

In this study, we investigated different types of silk-based scaffolds by varying fabrication methods, as a potential material of choice for bone tissue engineering applications [19, 26], with focus on hASCs as a cell source. Notably, the hASCs showed expression patterns of surface markers characteristic for mesenchymal stem cell ($CD105^+$, $CD73^+$, $CD90^+$, $CD45^-$, $CD44^-$) (Fig. 2A) consistent with that of the BM-MSCs, which have been successfully used

for engineering of bone [40]. The multi-lineage differentiation capability (adipogenic and osteogenic) was also verified and similar to that observed for BM-MSCs (Fig. 2B–D). Our previous studies confirmed the maintenance of high expression of the surface markers for hASC stemness and differentiation capability over several passages [32].

Four different types of silk scaffolds were investigated. Aqueous-based silk fibroin sponges were produced with three distinct pore size and morphology; Aq-250 structure used an average porogen size of 375 μm, which has been accepted as an optimal pore size for bone formation [41], Aq-500 aimed at resembling the pore size of native trabecular bone [42], and Aq-Lam, resembled the lamellar microstructure of bone [26]. In addition to aqueous-based scaffold, HFIP-400, another silk scaffold, which previously demonstrated rapid bone formation when cultured with BM-MSCs was also studied [21]. While groups Aq-250, Aq-500 and HFIP-500 present a spherical pore formed by salt-leaching, the Aq-Lam presents a structure where the pore walls form parallel lamellae, which are aligned in several directions (Fig. 3). The decellularized trabecular bone was used as a “gold standard”. The hASC osteogenic activity and bone formation among different scaffolds were directly compared.

The differences in silk scaffolds due to preparation methods did not affect the hASCs seeding efficiency (Fig. 4A) suggesting insignificant effect of solvent used and pore morphology on hASCs attachment. After cultivation for 7 weeks, cell number increased in all groups except Aq-Lam (Fig. 4B). Data suggest that cells have limited available space to proliferate once porosity, pore size and interconnectivity (Fig. 3 Bottom) are significantly inferior than those of aqueous-derived scaffolds with spherical pores (Aq-250 and Aq-500). Seeding efficiency in Aq-Lam group was not inferior than remaining groups, which may indicate that cells were efficiently seeded in the structure, and might have become saturated, limiting cell proliferation, and stimulating cell differentiation. Both Aq-250 and Aq-500 did not demonstrate significant difference regarding proliferation, which can be explained by contact inhibition [43]. Contrarily, proliferation data of HFIP-400 show a continuous increase throughout culturing period, but cell numbers by end of culture are not higher than other spherical-pore silk structures (Aq-250 and Aq-500). It seems that cells proliferated at a slower rate, which can be explained by its smoother pore surfaces, as has been reported [3].

Over 7 weeks, hASCs differentiated and expressed osteogenic markers in all groups but with different intensity. Bone tissue development for aqueous-based scaffolds, both small and large pore size (Aq-250 and Aq-500), was found to be similar. Pore size did not influence seeding efficiency or cell proliferation. Cell viability, morphology (Fig. 4C), and distribution throughout individual pores or entire scaffold were very similar between the two groups (Fig. 5 top). Bone proteins, such as osteopontin, bone sialoprotein and collagen type I, were produced and retained in the form of extracellular matrix in an analogous extent (Fig. 5). In addition, pore size did not affect amount of alkaline phosphatase production, calcium deposition and bone volume. Equilibrium moduli of Aq-250 and Aq-500 were also similar. We postulate that while smaller pores promote increased mechanical strength, on the other hand, the larger pores were associated with a more homogenous matrix [25], characteristics that may compensate the compressive capacity. Among all four silk scaffold groups in this study, both Aq-250 and Aq-500 were inferior.

Lamellar aqueous-based silk fibroin scaffolds (Aq-Lam) showed some interesting features. The equilibrium modulus was the highest among all silk scaffold groups, at beginning of culture, which might be due to the small inter-lamellar distance (25–100μm), but also demonstrated the most significant increase in mechanical properties after culture ($p<0.01$) (Fig. 7D). This reflects the significant calcium increase observed in this group ($p<0.05$) (Fig. 7B), and increased deposition of bone proteins such as OPN, BSP and Col I (Fig. 6).

Furthermore, the cells of Aq-Lam group expressed the most alkaline phosphatase activity at week 2 of culture (Fig. 7A), showing enhancement of osteogenic differentiation. Absolute values of calcium change and bone volume (Fig. 7B, 7C) though, were similar to those observed for Aq-250 and Aq-500 groups. This result may not be surprising as the native lamellar bone is generated more slowly than woven bone and is less mineralized [44].

Out of the four silk scaffold groups, HFIP-derived sponge supported superior hASCs osteogenic induction and bone-like tissue formation. The similarity of cell proliferation and morphology to aqueous-based scaffolds demonstrated that the higher silk concentration and HFIP solvent did not alter the abilities for hASCs to adhere and proliferate. However, HFIP-derived scaffolds enhanced hASCs deposition of matrix proteins (OPN, BSP, Col I) (Fig. 6) and mineralization, quantified by calcium retention in scaffold (Fig. 7B) and mineralized bone volume (BV) (Fig. 7C). According to microCT reconstruction of cultured constructs (Fig. 7E), mineral was evenly distributed throughout the scaffold in this group, showing homogenous osteogenic activity of hASCs. Regarding mechanical properties, although the equilibrium modulus of HFIP-based silk scaffold was higher than aqueous-based constructs with spherical pore, even from beginning of culture, possibly due to the higher concentration of silk material (Fig. 7D), among these three groups, HFIP-400 was the only group demonstrating significantly increase in mechanical properties from beginning to end of culture ($p<0.05$). This can be justified by the deposition of a more robust ECM, composed of both ECM-proteins and calcification, as discussed above.

The decellularized trabecular bone scaffolds have been used successfully in bone tissue engineering studies [32, 33, 45]. Although bone-forming structure and mechanical properties of the silk scaffolds were inferior to the trabecular bone scaffold, the osteogenic cellular activities in Aq-250 and Aq-500 groups were similar to bone scaffold and were enhanced in Aq-Lam and HFIP-400 groups (Fig. 6 and 7A).

Taken together, data collected in this study are consistent with the conceptual model shown in Fig. 8. Two distinguishable scaffold properties – scaffold architecture and mechanical stiffness – appear to affect bone formation (Fig. 8). First, scaffold stiffness is positively correlated with osteogenic differentiation of hASCs resulting in an increase in bone ECM secretion (Fig. 8A). The importance of mechanical properties in bone tissue engineering has been well established [19, 46]. Similar to previous findings, HFIP-derived silk fibroin scaffolds, which exhibited higher stiffness as compared to aqueous-based silk fibroin scaffolds, appear to provided a better platform for bone formation. Second, scaffold structure appears to alter cellular activities as well as bone tissue formation. Lamellar porous morphology is postulated to benefit hASC osteogenic differentiation into lamellar bone, which contains fewer cells, but higher mechanical properties once it is highly organized, while a spherical porous structure leads to the development of woven bone, which contains higher cellularity and mineral density but is far less organized [44, 47] (Fig. 8B).

Moreover, based on the extensive work already reported on bone tissue engineering with BM-MSC on silk scaffolds, and the data we present in this study, we may speculate that hASC are a good alternative cell source to BM-MSC for bone TE. For instance, at our research group, we have reported the outcomes of engineered bone grafts by culturing BM-MSC in similar HFIP scaffolds up to 5 and 10 weeks [6], and, even culturing in dynamic conditions by flow perfusion, bone related outcomes were less patent, than those obtained in the present study.

## 5. Conclusion

This study demonstrated the optimization potential of silk scaffolds in terms of structure (porosity, pore dimensions and pore geometry) and biomechanics for bone tissue

engineering applications. We demonstrated that human adipose derived stem cells (hASCs) interpret the extracellular environment, by responding differently to silk scaffolds' architecture, and producing bone-like extracellular matrix in a manner that appears to depend on structure and stiffness of scaffolds. Based on collected data, we have proposed a conceptual model that correlates bone tissue formation with architecture and stiffness of silk scaffolds, which emphasizes the importance of appropriate scaffold design when engineering bone.

## Acknowledgments

We gratefully acknowledge Rita Duarte for her help with experiments, and funding support of this work by the NIH (DE161525 and EB02520 to GVN), and the FCT PhD grant (SFRH/BD/42316/2007 to CC).

## References

1. Puppi D, Chiellini F, Piras AM, Chiellini E. Polymeric materials for bone and cartilage repair. Progress in Polymer Science. 2010; 35:403–440.
2. Salgado AJ, Coutinho OP, Reis RL. Bone tissue engineering: state of the art and future trends. Macromol Biosci. 2004; 4:743–65. [PubMed: 15468269]
3. Kim HJ, Kim HS, Matsumoto A, Chin IJ, Jin HJ, Kaplan DL. Processing windows for forming silk fibroin biomaterials into a 3D porous matrix. Australian Journal of Chemistry. 2005; 58:716–720.
4. Horan RL, Antle K, Collette AL, Huang YZ, Huang J, Moreau JE, Volloch V, Kaplan DL, Altman GH. In vitro degradation of silk fibroin. Biomaterials. 2005; 26:3385–3393. [PubMed: 15621227]
5. Saitow C, Kaplan DL, Castellot JJ. Heparin stimulates elastogenesis: Application to silk-based vascular grafts. Matrix Biol. 2011; 30:346–355. [PubMed: 21600981]
6. Bhumiratana S, Grayson WL, Castaneda A, Rockwood DN, Gil ES, Kaplan DL, Vunjak-Novakovic G. Nucleation and growth of mineralized bone matrix on silk-hydroxyapatite composite scaffolds. Biomaterials. 2011; 32:2812–20. [PubMed: 21262535]
7. Chao PHG, Yodmuang S, Wang XQ, Sun L, Kaplan DL, Vunjak-Novakovic G. Silk hydrogel for cartilage tissue engineering. J Biomed Mater Res B. 2010; 95B:84–90.
8. Yan LP, Oliveira JM, Oliveira AL, Caridade SG, Mano JF, Reis RL. Macro/micro Porous Silk Fibroin Scaffolds with Potential for Articular Cartilage and Meniscus Tissue Engineering Applications. Acta Biomaterialia. 2011 Accepted for publication.
9. Wang YZ, Kim HJ, Vunjak-Novakovic G, Kaplan DL. Stem cell-based tissue engineering with silk biomaterials. Biomaterials. 2006; 27:6064–6082. [PubMed: 16890988]
10. Murphy AR, Kaplan DL. Biomedical applications of chemically-modified silk fibroin. Journal of Materials Chemistry. 2009; 19:6443–6450. [PubMed: 20161439]
11. Hofmann S, Knecht S, Langer R, Kaplan DL, Vunjak-Novakovic G, Merkle HP, Meinel L. Cartilage-like tissue engineering using silk scaffolds and mesenchymal stem cells. Tissue Engineering. 2006; 12:2729–2738. [PubMed: 17518642]
12. Wang YZ, Kim UJ, Blasioli DJ, Kim HJ, Kaplan DL. In vitro cartilage tissue engineering with 3D porous aqueous-derived silk scaffolds and mesenchymal stem cells. Biomaterials. 2005; 26:7082–7094. [PubMed: 15985292]
13. Wang YZ, Blasioli DJ, Kim HJ, Kim HS, Kaplan DL. Cartilage tissue engineering with silk scaffolds and human articular chondrocytes. Biomaterials. 2006; 27:4434–4442. [PubMed: 16677707]
14. Mauney JR, Nguyen T, Gillen K, Kirker-Head C, Gimble JM, Kaplan DL. Engineering adipose-like tissue in vitro and in vivo utilizing human bone marrow and adipose-derived mesenchymal stem cells with silk fibroin 3D scaffolds. Biomaterials. 2007; 28:5280–5290. [PubMed: 17765303]
15. Kang JH, Gimble JM, Kaplan DL. In Vitro 3D Model for Human Vascularized Adipose Tissue. Tissue Eng Pt A. 2009; 15:2227–2236.
16. Lovett M, Eng G, Kluge JA, Cannizzaro C, Vunjak-Novakovic G, Kaplan DL. Tubular silk scaffolds for small diameter vascular grafts. Organogenesis. 2010; 6:217–224. [PubMed: 21220960]

17. Altman GH, Horan RL, Lu HH, Moreau J, IM, Richmond JC, Kaplan DL. Silk matrix for tissue engineered anterior cruciate ligaments. Biomaterials. 2002; 23:4131–4141. [PubMed: 12182315]
18. Chen JS, Altman GH, Karageorgiou V, Horan R, Collette A, Volloch V, Colabro T, Kaplan DL. Human bone marrow stromal cell and ligament fibroblast responses on RGD-modified silk fibers. Journal of Biomedical Materials Research Part A. 2003; 67A:559–570. [PubMed: 14566798]
19. Kim HJ, Kim UJ, Vunjak-Novakovic G, Min BH, Kaplan DL. Influence of macroporous protein scaffolds on bone tissue engineering from bone marrow stem cells. Biomaterials. 2005; 26:4442–4452. [PubMed: 15701373]
20. Meinel L, Karageorgiou V, Hofmann S, Fajardo R, Snyder B, Li CM, Zichner L, Langer R, Vunjak-Novakovic G, Kaplan DL. Engineering bone-like tissue in vitro using human bone marrow stem cells and silk scaffolds. Journal of Biomedical Materials Research Part A. 2004; 71A:25–34. [PubMed: 15316936]
21. Marolt D, Augst A, Freed LE, Vepari C, Fajardo R, Patel N, Gray M, Farley M, Kaplan D, Vunjak-Novakovic G. Bone and cartilage tissue constructs grown using human bone marrow stromal cells, silk scaffolds and rotating bioreactors. Biomaterials. 2006; 27:6138–6149. [PubMed: 16895736]
22. Vepari C, Kaplan DL. Silk as a biomaterial. Progress in Polymer Science. 2007; 32:991–1007. [PubMed: 19543442]
23. Nazarov R, Jin HJ, Kaplan DL. Porous 3-D scaffolds from regenerated silk fibroin. Biomacromolecules. 2004; 5:718–726. [PubMed: 15132652]
24. Kim UJ, Park JY, Li CM, Jin HJ, Valluzzi R, Kaplan DL. Structure and properties of silk hydrogels. Biomacromolecules. 2004; 5:786–792. [PubMed: 15132662]
25. Kim UJ, Park J, Kim HJ, Wada M, Kaplan DL. Three-dimensional aqueous-derived biomaterial scaffolds from silk fibroin. Biomaterials. 2005; 26:2775–2785. [PubMed: 15585282]
26. Oliveira AL, Sun L, Kim HJ, Hu X, Rice W, Kluge J, Reis RL, Kaplan DL. Designing silk-based 3D architectures with controlled lamellar morphology. Tissue Eng Pt A. 2008; 14:718–719.
27. Park SH, Gil ES, Shi H, Kim HJ, Lee K, Kaplan DL. Relationships between degradability of silk scaffolds and osteogenesis. Biomaterials. 2010; 31:6162–6172. [PubMed: 20546890]
28. Rockwood DN, Gil ES, Park SH, Kluge JA, Grayson W, Bhumiratana S, Rajkhowa R, Wang XG, Kim SJ, Vunjak-Novakovic G, Kaplan DL. Ingrowth of human mesenchymal stem cells into porous silk particle reinforced silk composite scaffolds: An in vitro study. Acta Biomaterialia. 2011; 7:144–151. [PubMed: 20656075]
29. Gimble JM, Guilak F, Bunnell BA. Clinical and preclinical translation of cell-based therapies using adipose tissue-derived cells. Stem Cell Res Ther. 2010; 1:19. [PubMed: 20587076]
30. Zuk PA, Zhu M, Mizuno H, Huang J, Futrell JW, Katz AJ, Benhaim P, Lorenz HP, Hedrick MH. Multilineage cells from human adipose tissue: implications for cell-based therapies. Tissue engineering. 2001; 7:211–28. [PubMed: 11304456]
31. Schaffler A, Buchler C. Concise review: adipose tissue-derived stromal cells--basic and clinical implications for novel cell-based therapies. Stem cells (Dayton, Ohio). 2007; 25:818–27.
32. Frohlich M, Grayson WL, Marolt D, Gimble JM, Kregar-Velikonja N, Vunjak-Novakovic G. Bone Grafts Engineered from Human Adipose-Derived Stem Cells in Perfusion Bioreactor Culture. Tissue Eng Pt A. 2010; 16:179–189.
33. Grayson WL, Bhumiratana S, Cannizzaro C, Chao PH, Lennon DP, Caplan AI, Vunjak-Novakovic G. Effects of initial seeding density and fluid perfusion rate on formation of tissue-engineered bone. Tissue Eng Part A. 2008; 14:1809–20. [PubMed: 18620487]
34. McIntosh K, Zvonic S, Garrett S, Mitchell JB, Floyd ZE, Hammill L, Kloster A, Halvorsen YD, Ting JP, Storms RW, Goh B, Kilroy G, Wu XY, Gimble JM. The immunogenicity of human adipose-derived cells: Temporal changes in vitro. Stem Cells. 2006; 24:1246–1253. [PubMed: 16410391]
35. Mitchell JB, McIntosh K, Zvonic S, Garretta S, Floyd ZE, Kloster A, Di Halvorsen Y, Storms RW, Goh B, Kilroy G, Wu XY, Gimble JM. Immunophenotype of human adipose-derived cells: Temporal changes in stromal-associated and stem cell-associated markers. Stem Cells. 2006; 24:376–385. [PubMed: 16322640]

36. Yu G, Wu X, Dietrich MA, Polk P, Scott LK, Ptitsyn AA, Gimble JM. Yield and characterization of subcutaneous human adipose-derived stem cells by flow cytometric and adipogenic mRNA analyzes. Cytotherapy. 2010; 12:538–46. [PubMed: 20380539]
37. Liu XWS, Sajda P, Saha PK, Wehrli FW, Guo XE. Quantification of the roles of trabecular microarchitecture and trabecular type in determining the elastic modulus of human trabecular bone. Journal of Bone and Mineral Research. 2006; 21:1608–1617. [PubMed: 16995816]
38. Mauck RL, Soltz MA, Wang CCB, Wong DD, Chao PHG, Valhmu WB, Hung CT, Ateshian GA. Functional tissue engineering of articular cartilage through dynamic loading of chondrocyte-seeded agarose gels. J Biomech Eng-T Asme. 2000; 122:252–260.
39. Gimble JM, Katz AJ, Bunnell BA. Adipose-derived stem cells for regenerative medicine. Circulation Research. 2007; 100:1249–1260. [PubMed: 17495232]
40. Gimble JM, Bunnell BA, Chiu ES, Guilak F. Concise Review: Adipose-Derived Stromal Vascular Fraction Cells and Stem Cells: Let's Not Get Lost in Translation. Stem cells (Dayton, Ohio). 2011; 29:749–754.
41. Karageorgiou V, Tomkins M, Fajardo R, Meinel L, Snyder B, Wade K, Chen J, Vunjak-Novakovic G, Kaplan DL. Porous silk fibroin 3-D scaffolds for delivery of bone morphogenetic protein-2 in vitro and in vivo. Journal of Biomedical Materials Research Part A. 2006; 78A:324–334. [PubMed: 16637042]
42. Keaveny TM, Morgan EF, Niebur GL, Yeh OC. Biomechanics of trabecular bone. Annu Rev Biomed Eng. 2001; 3:307–33. [PubMed: 11447066]
43. Huang, S.; Ingber, DE. From stem cells to functional tissue architecture. In: Sell, S., editor. Stem Cells Handbook. Humana Press Inc; Totowa, NJ: 2004.
44. McKenzie JA, Silva MJ. Comparing histological, vascular and molecular responses associated with woven and lamellar bone formation induced by mechanical loading in the rat ulna. Bone. 2011; 48:250–258. [PubMed: 20849995]
45. Grayson WL, Frohlich M, Yeager K, Bhumiratana S, Chan ME, Cannizzaro C, Wan LQ, Liu XS, Guo XE, Vunjak-Novakovic G. Regenerative Medicine Special Feature: Engineering anatomically shaped human bone grafts. Proc Natl Acad Sci U S A. 2009
46. Thomson, RC.; Shung, AK.; Yaszemski, MJ.; Mikos, AG. Principles of Tissue Engineering. Academic Press; 2000. Polymer Scaffold Processing.
47. Martin, RB.; Burr, DB.; Sharkey, NA. Skeletal tissue mechanics. Springer-Verlag New York, Inc; 1998.

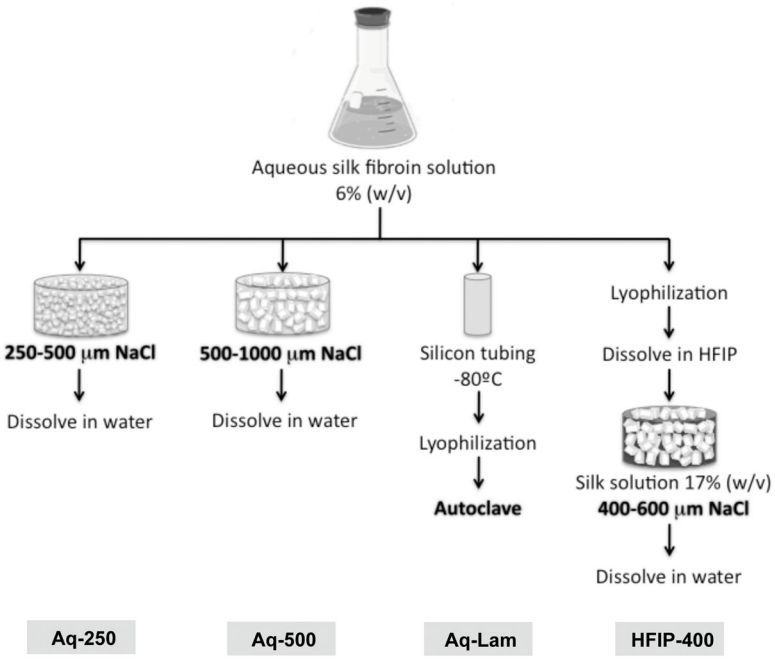


**Figure 1. Silk scaffold fabrication**

Silk fibroin is extracted from silk worm cocoons into an aqueous solution. Aqueous-based spherical pore scaffolds (**Aq-250** and **Aq-500**) are produced by salt-leaching method, where small (250–500 μm) or large (500–1000 μm) NaCl particles are used as porogen. Aqueous-based lamellar scaffolds (**Aq-Lam**) are produced by lyophilizing the frozen aqueous silk solution cast in a silicon tube. HFIP-derived porous scaffolds (**HFIP-400**) are developed by dissolving the lyophilized aqueous silk solution in HFIP solvent, to which NaCl particles (400–600 μm) are added to form the porous structure. NaCl particles used in salt-leaching method are further dissolved in water. Bold text represent step where β-sheet formation occur.

A

| Antigen | CD29 | CD105 | CD45 | CD34 | CD44 | CD73 | CD90 | PE Ctrl | FITC Ctrl | PBS Ctrl |
|---|---|---|---|---|---|---|---|---|---|---|
| Expression% | 99.03 | 98.82 | 11.87 | 93.94 | 12.7 | 88.48 | 93.46 | 8.1 | 7.4 | 7.1 |

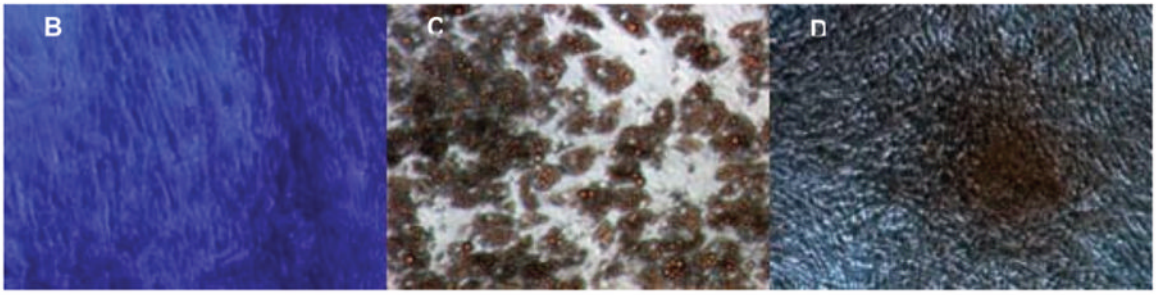


**Figure 2. Phenotypic characterization and evaluation of multipotency of human adipose stem cells**

**A)** Percentage of antigen expression in primary hASCs, **B)** Toluidine blue staining of undifferentiated stromal cells, **C)** Oil red O staining for adipogenesis, **D)** Alizarin red staining for osteogenesis.

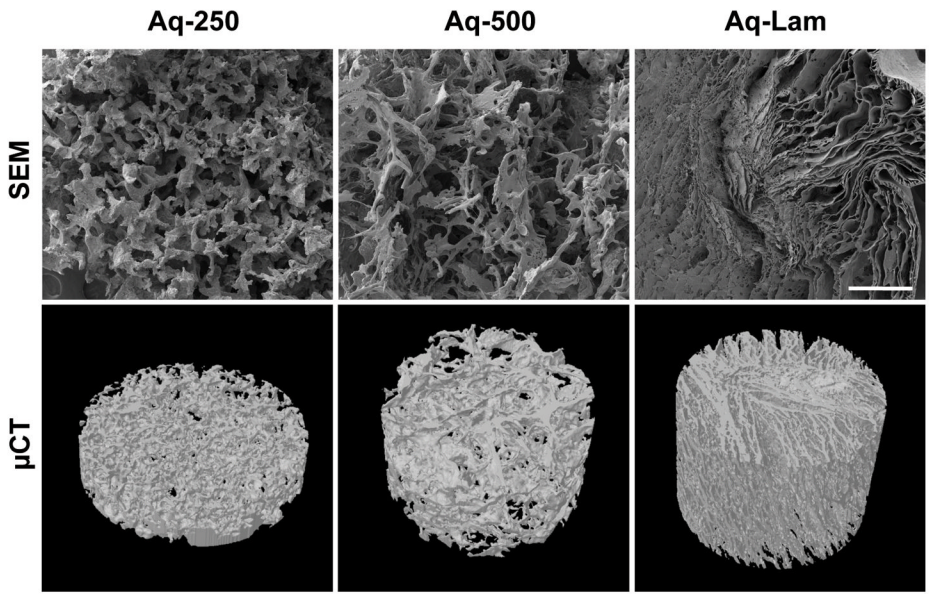


| | Aq-250 | Aq-500 | Aq-Lam |
|---|---|---|---|
| Porosity (%) | 75.95 ± 1.55 | 86.62 ± 0.84 | 64.25 ± 8.82 |
| Interconnectivity (%) | 90.97 ± 3.02 | 97.83 ± 0.61 | 63.25 ± 21.13 |
| Average pore size (µm) | 139.74 ± 30.05 | 254.32 ± 13.64 | 126.24 ± 48.16 |
| Trabeculae thickness (µm) | 59.98 ± 5.88 | 56.51 ± 3.55 | 63.13 ± 20.47 |

**Figure 3. Aqueous-based silk fibroin scaffolds characterization**

**Top row)** Scanning electron microscopy (SEM) images of Aq-250, Aq-500 and Aq-Lam scaffolds demonstrating pore morphology and wall surface. Scale bar = 500 µm. **Middle row)** Micro-computed tomography (µCT) 3D reconstruction of silk fibroin scaffolds. **Bottom)** Morphometric parameters obtained by µCT analysis.

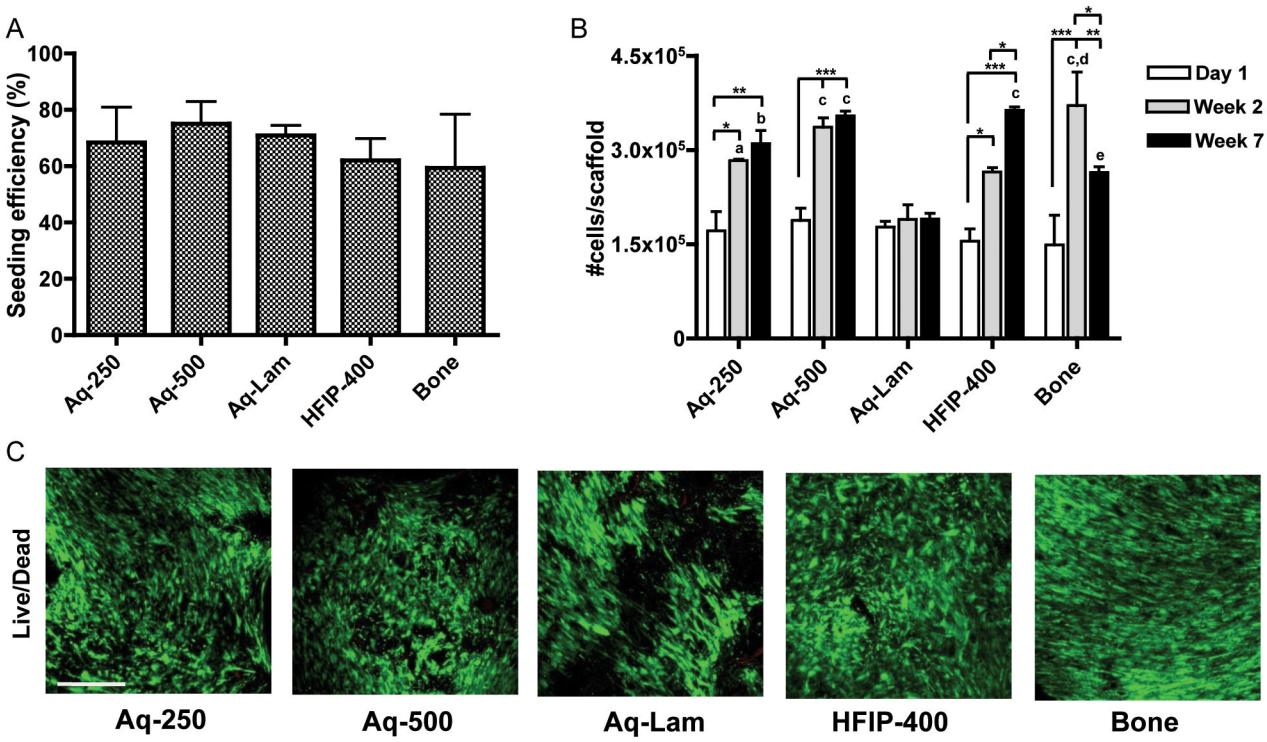


**Figure 4. Cell viability and proliferation**

**A)** Cell seeding efficiency. No significant differences were observed between groups. **B)** Cell proliferation evaluated by changes in the number of cells per scaffold. *p<0.05, **p<0.01, ***p<0.001; **a** p<0.05, **b** p<0.01, **c** p<0.001 to Aq-Lam; **d** p<0.05 to Aq-250 and HFIP-400; **e** p<0.05 to Aq-500 and HFIP-400; **C)** Cell viability (Live/Dead assay) after 7 weeks of culture. Scale bar = 200 μm.

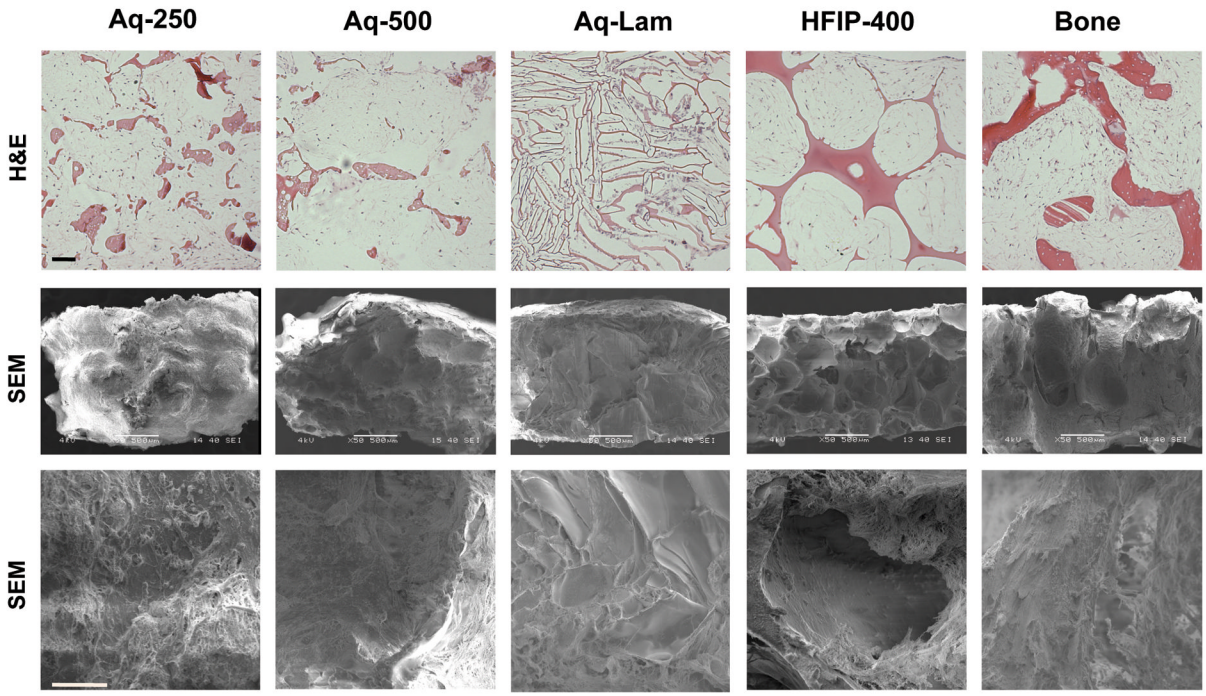


**Figure 5. Scaffold structure**

Constructs were analyzed after seven weeks of culture. Top row: Hematoxylin & Eosin (H&E) staining, scale bar = 200 μm; Middle row: Scanning electron microscope (SEM) images 50x, scale bar = 500 μm. Bottom row: SEM images 400x, scale bar = 50 μm.

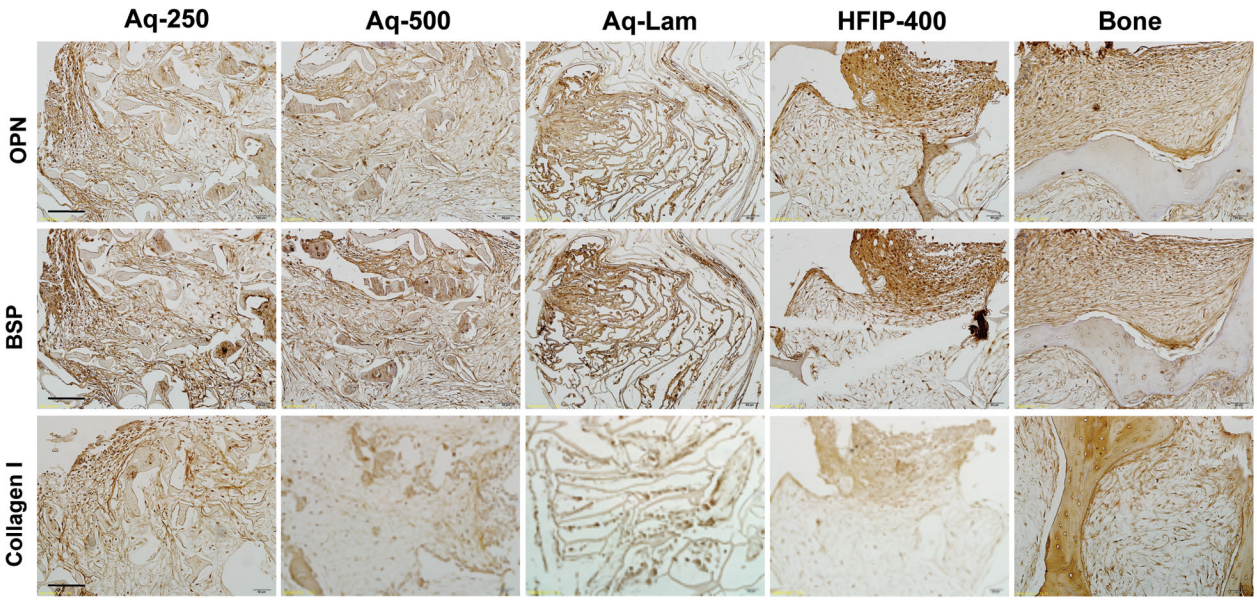


**Figure 6. Accumulation of bone matrix proteins in tissue constructs**

Data are shown after 7 weeks of culture. Top row: Osteopontin (OPN); Middle row: Bone Sialoprotein (BSP); Bottom row: Collagen type I. Scale bar = 100 μm.

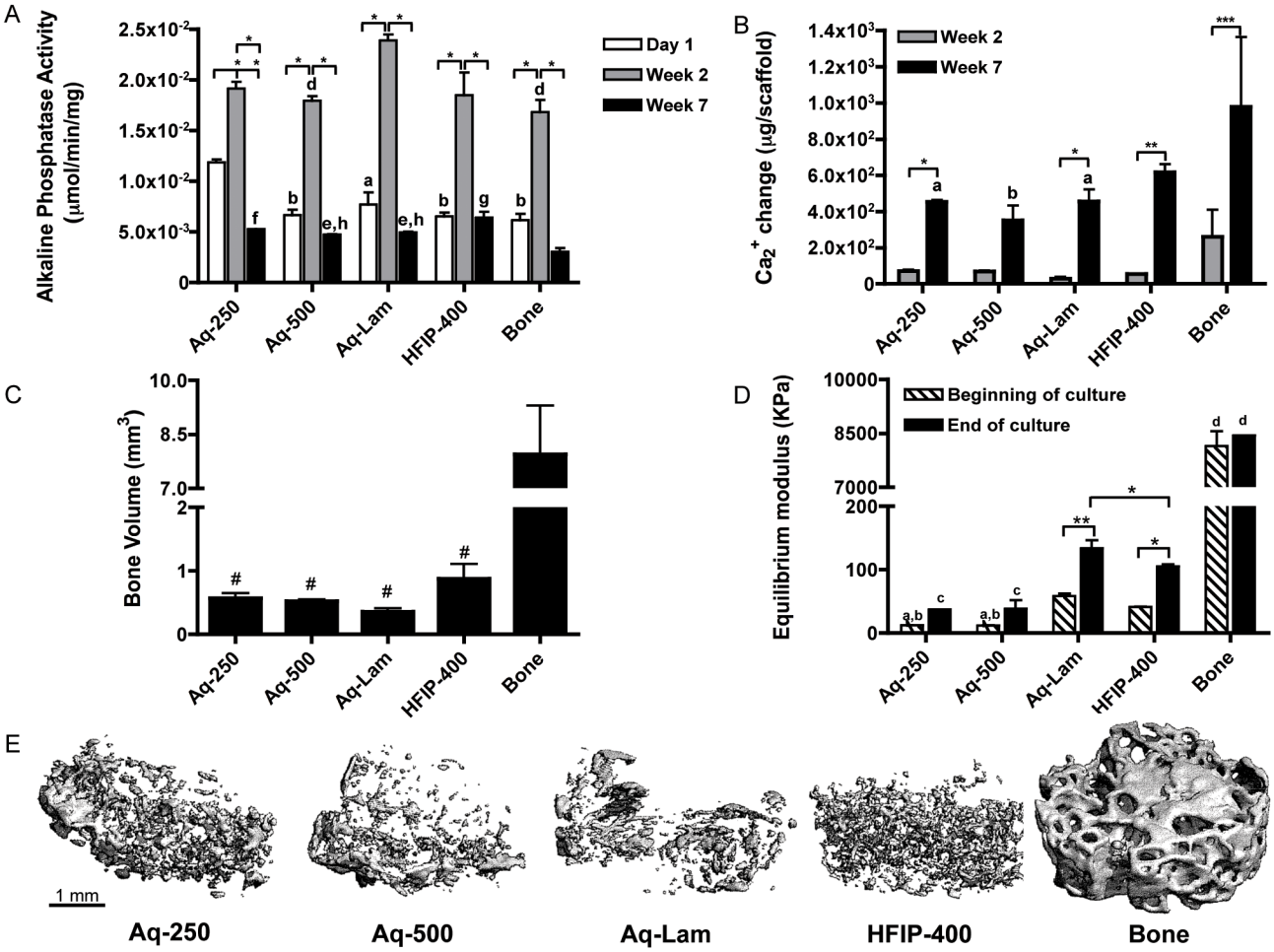


**Figure 7. Biochemical and mechanical characterization of constructs**

**A)** Alkaline phosphatase activity *p<0.001; **a** p<0.05, **b** p<0.01 to Aq-250; **d** p<0.05 to Aq-Lam; **e** p<0.05, **f** p<0.01, **g** p<0.001 to Bone. **B)** Calcium change from day 1 measured at two and seven weeks of culture, *p<0.05, **p<0.01, ***p<0.001; **a** p<0.05, **b** p<0.01 to Bone. **C)** Bone volume (BV) of constructs at week 7 # p<0.05 to Bone. **D)** Equilibrium modulus at beginning and end of culture *p<0.05, **p<0.01; **a** p<0.05 to HFIP-400, **b** p<0.001 to Aq-Lam, **c** p<0.001 to HFIP-400 and Aq-Lam, **d** p<0.001 to all other groups. **E)** μCT reconstruction images of constructs after 5 weeks of culture. Scale bar = 1 mm.

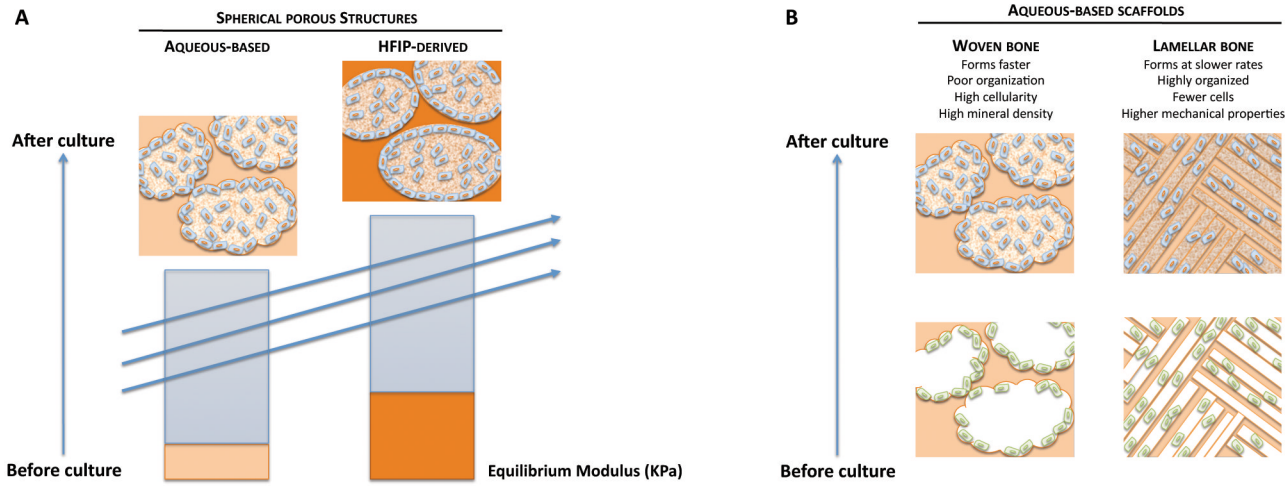


**Figure 8. Proposed mechanism of regulation of bone formation by scaffold architecture and stifness**

**A) Scaffold mechanics.** Mechanically stronger HFIP-derived silk scaffolds promote osteogenic differentiation of hASCs to result in increased bone volume (BV), calcium content and bone protein deposition, as compared to aqueous-based scaffolds. **B) Scaffold architecture.** Sponge like architecture with spherical pores serves as a template for the formation of woven bone, while a lamellar porous architecture serves as a template for the formation of lamellar bone.